SPATIAL PATTERNS OF SEDIMENT ACCUMULATION ON A HOLOCENE CARBONATE TIDAL FLAT, NORTHWEST ANDROS ISLAND, BAHAMAS

EUGENE C. RANKEY*
Department of Geology and Atmospheric Sciences and Virtual Reality Applications Center, Iowa State University, Ames, IA 50011, U.S.A.

ABSTRACT: **To characterize spatial patterns of sedimentation and analyze the morphology of part of the modern tidal flats of northwest Andros Island in the Bahamas, this study integrated remote sensing, geographic information systems (GIS), and carbonate sedimentology. The fundamental data are a Landsat TM image that has been classified to create a thematic map of eight subfacies, interpreted to represent a distinct tidal-flat subenvironment such as adjacent marine, exposed levee-beach ridge, pond, and algal marsh. Spatial statistics of the thematic map characterize the patterns of sediment accumulation.**

Quantitative analysis highlights several interesting results concerning subfacies character and distribution: (1) of the eight mapped subfacies, low algal marsh is most widespread, representing 27.5% of the total area, whereas exposed levee-beach ridge is the least widespread, accounting for 10% of the area; (2) the patches of different subfacies have different shape complexities, with low algal marsh, high algal marsh, and mangrove ponds being the least complex and exposed levee-beach ridge being the most complex; (3) Markov chain analysis suggests that lateral transitions between different subfacies are highly ordered; and (4) frequency distribution of subfacies patch area and lacunarity (gap size distribution) data exhibit power law relationships over several orders of magnitude, consistent with fractal characteristics.

The fractal nature of patch size and gaps between facies illustrate that on this tidal flat neither the size nor the spatial distribution of subfacies has a characteristic scale. This statistical behavior is consistent with the presence of self-organization, or emergence of pattern in the absence of a template or external forcing. The statistical self-organization on the tidal flat is the cumulative expression of local processes, but it becomes apparent only through analysis of the whole system. These results are inconsistent with models suggesting that tidal flats include a migrating complex of randomly distributed, randomly sized subenvironments. Ancient successions that include random patterns may reflect the more pronounced influence of forces external to the sedimentary system, instead of an absence of those forces.

INTRODUCTION

In the 17th century, Nicolas Steno recognized that beds exhibit a finite lateral extent. From this observation, he formulated the Principle of Lateral Continuity, stating that strata originally extend in all directions until they end by thinning, ending against a barrier, grading into another type of sediment, or were eroded. Many stratigraphic studies of peritidal carbonate successions have attempted to evaluate the lateral continuity of parasequences (e.g., Koerschner and Read 1989; Hardie et al. 1991), but in only a few studies have individual beds been traced (e.g., Pratt and James 1986; Waters et al. 1989; Cloyd et al. 1990; Adams and Grotzinger 1996). The importance of documenting and measuring spatial properties is highlighted by the inferred importance of the ''facies mosaic'' that has been interpreted on the basis of study of ancient tidal-flat successions (Cloyd et al. 1990; Kozar et al. 1990; Goldhammer et al. 1993; Diedrich and Wilkinson 1999; Wilkinson et al. 1999), and by the commonly abrupt and pronounced lateral changes that have been documented in cross sections from some ancient carbonate successions in which individual beds have been carefully traced (for example, Laporte 1967; Pratt and James 1986; Cloyd et al. 1990; Satterley 1996; Adams and Grotzinger 1996). Such descriptions of complex thickness and facies patterns have led some workers to hypothesize that ancient peritidal successions represent deposition from ''randomly'' distributed suites of subenvironments (Wilkinson et al. 1997, 1999).

The stratigraphic record reflects the cumulative effects of sediment accumulation through time. Therefore, describing and characterizing the distribution and spatial patterns of sediment accumulations at one time should provide insights into the inherent complexity that could be part of analogous ancient systems. Previous studies of modern environments have been useful in providing criteria for recognizing and interpreting ancient facies and developing predictive facies models (e.g., Shinn et al. 1969; Shinn 1973a, 1973b; Enos 1977; Hardie et al. 1977; Harris 1979), but most have focused on small-scale processes active in these environments and the sedimentologic products. Thorough quantitative description of the spatial distribution of sediment accumulation, and the relation to sedimentologic processes, has not been the focus of any of these studies.

The primary purpose of this study is to statistically describe the patterns of sediment accumulation on the modern carbonate tidal flat of northwest Andros Island, Bahamas. The goals of this paper are: (1) to illustrate how remote-sensing data can be used to create accurate thematic maps of modern carbonate depositional systems, (2) to demonstrate how the heterogeneity of these systems can be quantitatively measured and analyzed using geographic information systems (GIS) and statistical tools, (3) to interpret how depositional processes and sedimentologic patterns are related on this tidal flat, and (4) to comment on some potential implications of these results for the study of ancient peritidal successions.

BACKGROUND

Study Area and Previous Work

The modern carbonate tidal flat on the northwest coast of Andros Island, Bahamas, is up to 5 km wide and $>$ 70 km long parallel to the western side of the island (Fig. 1) and includes three very general geomorphic zones: (1) a marginal marine region; (2) a channeled intertidal belt that is alternately flooded and exposed with the tides; and (3) a marsh that is mostly above mean high tide (Shinn et al. 1969; Gebelein 1974; Hardie 1977; Hardie and Shinn 1986). Each of these areas can be further subdivided on the basis of their position relative to tides, sediment types and biota, and depositional processes, and include areas such as beach ridges, ponds, and channels. Previous studies (Shinn et al. 1969; Gebelein 1974; Hardie 1977) of Andros Island tidal flats included detailed sedimentologic analysis and qualitative mapping of sedimentary environments using traverses and aerial photography.

Several workers have utilized remotely sensed data to study modern carbonate depositional systems (e.g., Harris and Kowalik 1994; McNeill 1998; Gischler and Lomando 1999). These studies have focused on qualitative description of the spatial depositional patterns or performed only a limited set of measures (e.g., facies dimensions, McNeill 1998).

Wilkinson et al. (1999) provided some of the first quantitative data on the characteristics of facies areas of Holocene carbonate sediments in the Bahamas and Florida. For their study, they utilized the maps of Enos (1974) that defined 90 areas with distinct sedimentologic properties (facies units

* Present Address: Division of Marine Geology and Geophysics, Rosenstiel School of Marine and Atmospheric Science, University of Miami, 4600 Rickenbacker Causeway, Miami, Florida 33149.

JOURNAL OF SEDIMENTARY RESEARCH, VOL. 72, NO. 5, SEPTEMBER, 2002, P. 591–601
 1527-1404/02/072-591/$03.00

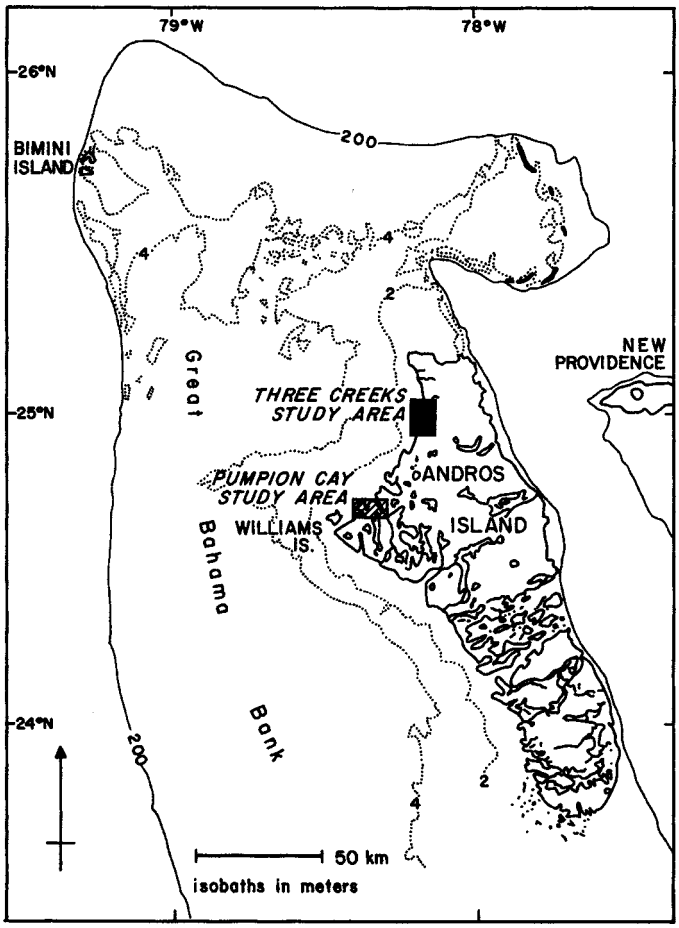

FIG. 1.—Location map, from Hardie (1977). The study area is in the area of the black box and corresponds with Hardie's Three Creeks study area.

or lithotopes) in the 197,097 km² study area. The results of their study included a description of exponential frequency distributions that they ascribed to Poisson processes of sediment accumulation. This study extends these results, analyzes a smaller area in more detail (n = 1278 subfacies units in ~ 70 km²) and includes a more systematic and integrated study of spatial patterns and their relation to sedimentary processes.

Spatial Statistics

Spatial statistics are a quantitative set of metrics that have been used extensively in the field of landscape ecology to describe and evaluate patterns and processes in ecology, landscape architecture, and land use (see reviews and compilations by Turner and Gardner 1991; Farina 1998).

The fundamental unit of analysis in this study is the *patch*, a discrete, relatively homogeneous spatial domain distinguished by properties unique from surrounding patches. Patches with similar properties are said to belong to the same *class*. In this study, a patch is defined as an area with distinct spectral properties (as defined by Landsat TM data), interpreted to reflect distinct sedimentologic properties. A *landscape* is an area that includes a group of patches; in this study, the landscape is the study area.

Landscape composition refers to the kinds, amounts, and properties of patches within a landscape, without consideration of their location (Turner and Gardner 1991). Metrics of landscape composition for each patch include attributes such as size, perimeter, and shape complexity, as well as characteristics of a class of patches such as mean size or mean shape complexity.

Landscape configuration measures the character of patches within the landscape with explicit reference to their spatial location (Turner and Gardner 1991). These measures quantify attributes such as distribution of patch types relative to other patch types, an environmental boundary, or any other feature (for example, minimum distance to a patch of the same class, average distance to nearest neighbor, complexity of boundary). These types of measures are important because environments, processes, and organisms are not isolated but are influenced by and linked to adjacent environments.

Quantitative Methods

The fundamental input for these analyses is a Landsat 5 Thematic Mapper (TM) image acquired April 29, 1986. The Landsat system was designed to measure reflected radiation, a parameter that varies with wavelength and the reflecting material. In principle, by examining the characteristics of reflections in different wavelengths, the reflecting surface can be characterized. These Landsat data have a spatial resolution of 28.5 m × 28.5 m.

To separate areas with different spectral signatures, data were analyzed using unsupervised classification (isoclass clustering analysis process in ERMapper), a statistical technique that assigns observations (in this case pixels) to more or less homogeneous classes that are distinct from other classes (Davis 1986). Statistically, the technique seeks to maximize variability between classes while minimizing variability within classes.

Unsupervised classification of Landsat TM bands 1–5 and 7 provided a preliminary thematic map of environments. Initially, the classification was run to generate 5, 6, 7, 8, 10, 15, 20, 25, and 50 classes. When compared with aerial photographs and published maps of Hardie (1977), the maps of 5–7 classes lumped subenvironments, whereas maps with greater than 10 classes could not be interpreted sedimentologically given available data.

The eight-class thematic map derived from unsupervised classification was utilized as input for a maximum likelihood supervised classification. Supervised classification is a statistical technique in which the geographic locations at which certain classes occur are known beforehand, and data from these areas are used to define ''training regions'' that provide guidelines for assigning other pixels to classes. The use of supervised techniques is advantageous because it provides measures that can be used to check the quality of classification. One such measure is posterior probability, a description of the likelihood that a pixel belongs to each class. For the analyses of these data, each class had median posterior probabilities of falling in the initial (input) class of greater than 86%, and only one was less than 92.5%, suggesting that there is internal consistency and separation among classes.

Resultant maps were checked against the maps of Hardie (1977), aerial photographs, and ultra-high-resolution (1 m) satellite images for validation (these maps and images were used earlier to define the optimal number of classes, not for calibration, and thus remain independent data) and interpreted in the context of depositional subenvironments. Because the maps of Hardie (1977) were not geospatially registered, it was not possible to measure classification accuracy quantitatively (cf. Andrefouet and Claereboudt 2000). Qualitative results (illustrated below) suggest that maps provide an accurate assessment of depositional subenvironments (given their resolution). Following validation, these thematic maps were filtered using a classification smoothing filter (the ''majority'' filter in ERMapper), then transformed from a raster image to a vector format and analyzed in ARC/INFO. Quantitative measures were exported to a statistics program for analysis.

THEMATIC MAP OF SEDIMENTS

Satellite images and the final thematic map of sediments are illustrated on Figure 2. Comparison of the thematic map with the ultra-high-resolution satellite imagery (Figs. 2, 3) and the previous, ground-truthed maps of Hardie (1977) (Fig. 3) suggest that maps provide a good representation of

the large-scale patterns of surface sediments, although the 28.5 m^2 pixel size of the Landsat data preclude imaging of smaller features. The effects of pixel size on observed patterns can be pronounced, typically with an increase in heterogeneity with an increase in resolution (King 1987; Obeysekera and Rutchey 1997). These effects are the focus of considerable research, however, and detailed consideration is beyond the scope of this report.

One potential limitation of this analysis is that the classification defines areas with similar spectral signature, not similar subenvironments. In this regard, the classes displayed in Figure 2C are not, by definition, subenvironments. Instead, they are ''spectral facies'' or ''spectral classes,'' areas with similar spectral response caused by similar ecologic, sedimentologic, or hydrologic features. My assumption is that because environment and sedimentology are so closely linked on the tidal flat (Shinn et al. 1969; Hardie 1977) patterns revealed by the data approximates the distribution of environments, as validated by comparisons in Figures 2 and 3. In this paper, to make distinctions clearer the name of the interpreted subenvironment is used in describing classes.

Channels were not spectrally unique because as the larger channels shallow and narrow, their spectral characteristics change, making objective spectral classification difficult. Because of this limitation, channels were not separated explicitly as a distinct class. Even where below resolution, however, their effects can commonly be detected by the exposed levee-beach ridges subfacies extending outward, away from the larger channels (Figs. 2, 3C). The significance of the channels is not ignored, however; in a later section, their influence is described and quantified.

DESCRIBING AND ANALYZING SEDIMENT ACCUMULATION PATTERNS

The Abundance, Size and Shape Complexity of Classes—Landscape Composition

Not all patches are present in equal abundance (Fig. 4). By total area, for patches within the channeled belt, the low algal marsh is most widespread, including 27.5% of the area, whereas the high algal marsh and exposed levee-beach ridge account for 11% and 10% of the area, respectively. By number, patches of the mangrove pond are most common ($n = 332$), whereas patches of the open pond-shallow marine subfacies are least common ($n = 122$). Percentage of the landscape is not correlated with the number of classes ($R^2 = 0.05$).

The characteristics of subfacies area can be described by examining exceedance probability versus area, both on log scales. Exceedance probability is defined as $P = m/(n + 1)$, where m = ranking from smallest to largest and n = number of samples, and represents the cumulative probability $P[X \geq x]$ of a given patch of area X having an area larger than x. In other words, the data plotted on the figure represent the probability (y axis) that a given patch will be of area equal or greater than a given area (x axis).

Given the power function $g(x) \alpha ax^d$, where $g(x)$ is the exceedance probability, a and d are constants, and x = patch area, we can quantify the relations between exceedance probability and patch area. Figure 5A illustrates data for all subfacies, plotted with different symbols, with two end-member power-law relationships illustrated. The relationship between area and exceedance probability for all illustrated subfacies can be described by power laws, each with $R^2 > 0.95$ ($p < 0.0001$), with d ranging from 0.50 to 0.69. These good power-law relationships (cf. Carlson and Grotzinger 2001) show that the data on area vs. exceedance probability for each subfacies are scale invariant, or statistically self-similar, across several orders of magnitude (Rodriguez-Iturbe et al. 1992; Turcotte 1997; cf. Wilkinson et al. 1999). Following Turcotte (1997, p. 16–17), these power-law relations and self-similar characteristics are defined as ''fractal.'' The corresponding fractal dimensions are equal to the slope plus the Euclidian dimension (here 2, because these are two-dimensional bodies); therefore, the fractal dimension (D) of channeled belt subfacies ranges from 1.32 (low algal marsh) to 1.50 (open pond-shallow subtidal) (Fig. 5).

A lower slope for a subfacies indicates that, for a given probability (y axis), a given patch probabilistically will have an area (x axis) greater than that for a subfacies with a higher slope. For example, for the low algal marsh (slope = −0.69; $D = 1.31$), there is a 10% probability (exceedance probability = 0.10) that a given patch is larger than ~ 14,600 m^2 (~ $10^{4.16}$) in area, whereas for the open pond-shallow subtidal (slope = −0.50; $D = 1.50$), there is a 10% probability that the size of a given patch is greater than ~ 64,900 m^2 (~ $10^{4.81}$). In other words, subfacies with lower slopes (and higher D) are (probabilistically) characterized by patches of greater area.

Data for several subfacies have a change in trend at areas of ~ 100,000 (10^5) m^2, and in some cases, the data might be more accurately described by two lines (e.g., be bifractal). The most pronounced example is data from the exposed levee-beach ridge. In these data (Fig. 5B), patches with areas < 100,000 m^2 have a fractal dimension of 1.56 ($R^2 = 0.95$, $p < 0.0001$), whereas those > 100,000 m^2 have a fractal dimension of 0.75 ($R^2 = 0.97$, $p < 0.0001$), a pronounced difference. These changes suggest the influence of at least two different geomorphic processes (cf. Kent and Wong 1982), and that something ''limits'' the extent of patches > 100,000 m^2 relative to that predicted by the characteristics of patches < 100,000 m^2, leading to smaller areas (lower D).

What might cause this bifractal nature? If we examine the distribution of ''small'' patches of this class, an interesting result emerges. Of those patches < 100,000 m^2, 89% (106/119) occur away from the coast (exposed levees) but of patches > 100,000 m^2, 64% (7/11) fall along the coast. The bifractal nature therefore appears to be related to the fact that this class includes both exposed levees and beach ridges, areas with geomorphically distinct processes (but similar spectral character).

There are several means by which the characteristics of shape complexity can be described. In this study, two different parameters are utilized: the ratio of maximum axis length to minimum axis length (RLSA) and interior circumscribed circle (ICC) (defined below). These parameters do not measure shape as morphometric analysis would, and two patches with similar shape complexity can have vastly different shapes. Additionally, neither metric captures all aspects of shape complexity, but each provides slightly different and useful information. Defining accurate measures for shape complexity is an active area of research (Farina 1998; Bryson and Mobolurin 2000; Saura and Martinez-Millan 2001), and no one metric is universally accepted or uniquely diagnostic of a particular process.

The ratio between the longest axis of the patch and the shortest axis (RLSA) of the patch is a dimensionless metric in which a higher ratio means that the patch is more elongate and a lower ratio suggests a more equant shape. All data for all facies are illustrated in Fig. 6. Comparison among channeled-belt subfacies reveals that the mean RLSA for exposed levee-beach ridge is highest (2.90, more elongate); lowest mean RLSA are in low algal marsh (2.25, more equant) and mangrove pond (2.20, more equant).

Another measure of shape complexity is interior circumscribed circle (ICC), which compares patch area with the area of the largest circle that fits within a patch, normalized to the area of the patch. It is defined as

$$\text{ICC} = (\text{patch area} - \text{area of largest circle within patch})/\text{patch area}$$

ICC is a measure of how much a shape deviates from that of a perfect circle, with 0.0 being a circle and higher numbers (approaching 1.0) reflecting more complex shapes. The value of ICC can be thought of as the proportion of the patch that lies outside the largest enclosed circle. ICC characterizes shape complexity relative to a circular standard; it does not describe the morphology and it is *not* sensitive to changing morphology.

Like patch area, shape complexity factor (ICC) varies among classes (Fig. 6). Whereas the exposed levee-beach ridge is characterized by a high

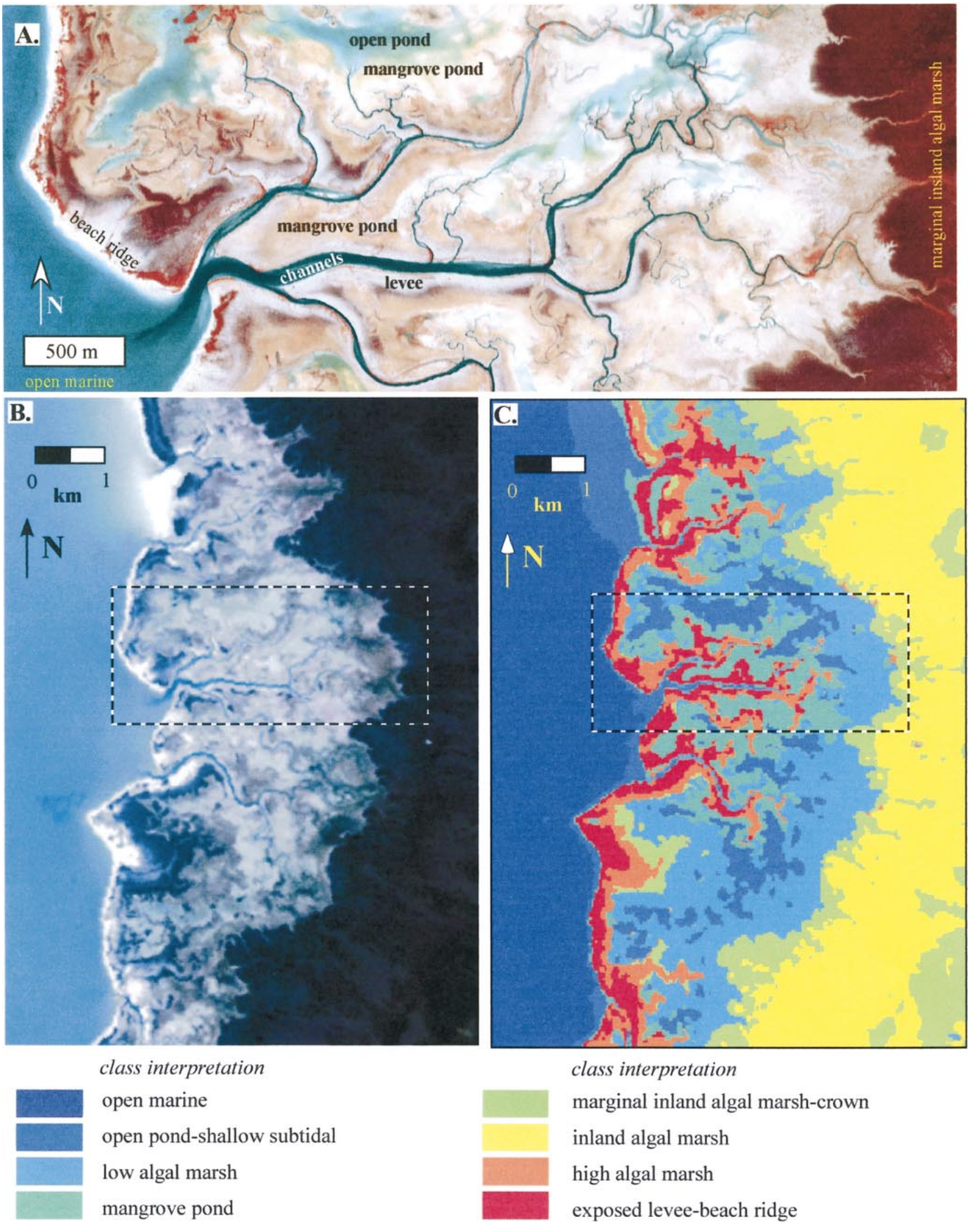
A.
open pond
mangrove pond
mangrove pond
beach ridge
channels
levee
marginal insland algal marsh
N
500 m
open marine
B.
0
1
km
N
C.
0
1
km
N
class interpretation
open marine
open pond-shallow subtidal
low algal marsh
mangrove pond
class interpretation
marginal inland algal marsh-crown
inland algal marsh
high algal marsh
exposed levee-beach ridge

mean shape complexity factor (0.57), mangrove pond and high algal marsh have lowest mean shape complexity (0.47 and 0.46, respectively).

These two shape measures are not strongly correlated (Fig. 6). This lack of correlation illustrates that these metrics capture different aspects of shape (elongation versus irregularity) and shows that more irregular patches (higher ICC) can be equant or elongate (a wide range of RLSA) and that more equant patches can have a range of shape complexities.

Patches in a Spatial Context—Landscape Configuration

Although the landscape composition characteristics of different patch types are interesting, they do not place the information in a spatial context. Because patches do not occur in isolation, but are influenced by their neighbors and setting, landscape configuration is important.

Order in Bounding Subfacies—Markov Chain Analysis.—We can characterize the landscape configuration by measuring the disorder of bounding subfacies of each subfacies by means of Markov chain analysis (Carr 1982; Davis 1986). This analysis characterizes the complexity of subfacies transitions and tests whether a system contains non random transitions. A system with more than two discrete, mutually exclusive states is said to contain a first-order Markov property if ''the state of the system at time t_n is influenced by or dependent on the state of the system at time t_{n-1}, but not the previous history that led to the state at time t_{n-1}'' (Carr 1982, p. 905). Instead of assessing the system in time, we can assess it in space, asking whether the class at a pixel is influenced by the class of the adjacent pixels (in this case, in four nondiagonal cells). This step is done by comparing the observed transition matrix with the matrix of expected values (e.g., if the pattern were random). For this study, we utilized embedded Markov chain analysis, in which a given class does not follow itself.

For embedded Markov chain analysis of this map (Fig. 2C), with 41 degrees of freedom (d.f. $= (m - 1)^2 - m$, where m = the number of classes, eight in this example; Davis 1986), the chi-squared value is 55489, extremely high compared to the chi-squared of 77 that is significant at $p = 0.0005$. At this high value, we can reject the hypothesis that lateral transitions are random with a significance of $p =$ essentially zero. Therefore, we can emphatically reject the hypothesis that lateral transitions among subfacies are random.

Distribution of Gaps between Patches—Lacunarity Analysis.—An alternative means of characterizing landscape configuration is through lacunarity analysis, a technique that measures the texture or ''gappiness'' of a geometric structure (Allain and Cloitre 1991; Plotnick et al. 1993). Lacunarity measures the degree of similarity of parts of a geometric structure to one another at a given scale. Lacunarity here is calculated using the techniques of Plotnick et al. (1993), in which an $r \times r$ box is placed over the upper left corner of the area of interest (the study area). The number of pixels (referred to as the box mass) filled with the subfacies of interest are counted. The box is then moved one column to the right, and the process is repeated, until all rows and all columns have been counted. This process is repeated for box sizes of gradually increasing size, until the box represents the entire landscape. The result is a frequency distribution of box masses for that box size. The probability distribution $Q(S,r)$ of the number of boxes with size r containing box mass of S is calculated by $Q(S,r) = n(S,r)/N(r)$, where $n(S,r)$ is the number of boxes with size r containing box mass of S, and $N(r)$ is the number of boxes of size r.

The first (mean) and second (variance) moments of the distribution are then calculated:

$$Z1 = \sum SQ(S, r) \qquad Z2 = \sum S2Q(S, r)$$

And lacunarity is defined as

$$\Lambda(r) = Z2/(Z1)^2$$

In this study, each subfacies was considered separately, and each pixel was labeled as either present or absent. Contiguous patches of pixels in which the subfacies under consideration were absent were considered ''gaps,'' and contiguous groups of pixels in which subfacies were present were ''patches.'' Landscapes in which gaps between patches are similar are made of homogeneously distributed geometric objects, and the landscape has low lacunarity. For a given box size, as the variance of the gaps between patches approaches zero, lacunarity approaches one. In contrast, landscapes with a range of gap sizes are more heterogeneous and have high lacunarity. Lacunarity can be utilized as a *scale-dependent* measure of texture, but it is best described across a range of scales (Plotnick et al. 1993).

Lacunarity data are displayed as plots of lacunarity vs. area, both on a log scale. Allain and Cloitre (1991) and Plotnick et al. (1993) noted that the lacunarity curve for a self-similar fractal is a straight line, indicating a power-law relationship, with the slope of the line equal to the fractal dimension minus the Euclidian dimension (here 2, because we are analyzing in map view). The lacunarity curves for all channeled-belt subfacies (e.g., all subfacies of this study except open marine and the inland algal marsh) approximate lines over areas up to the scale of the study area with the coefficient of determination (R^2) between log (lacunarity) and log (area) greater than 0.94 ($p < 0.0001$). These parameters suggest that the distribution of gaps is statistically self-similar and scale independent across several orders of magnitude (Fig. 7). The non-self-similar inland algal marsh data (from outside the channeled belt) are illustrated in Figure 7G for comparison.

Although all subfacies show self-similarity, there are differences among subfacies. The fractal dimensions across the entire spatial size scale of this study ranges from 1.67 (exposed levee-beach ridge) to 1.77 (low algal marsh) (Fig. 7), with lower fractal dimensions (higher slope) representing larger and more variable gaps. Likewise, although these R^2 values are statistically significant across the entire range of scales of this study (cf. Carlson and Grotzinger 2001), for some subfacies better fits can be developed if segments of the data are used. For example, for mangrove pond data (Fig. 7C) at box sizes $< 1.6 \times 10^6$ m^2, the coefficient of determination (R^2) between log (lacunarity) and log (area) is 0.997 ($p < 0.0001$), almost a perfect fractal, with $D = 1.80$. At larger scales, the power-law relationship is less well developed. For other subfacies such as the exposed levee-beach ridge and the high algal marsh, a single power-law relationship appears to be appropriate across the whole range of scales.

DISCUSSION: RELATIONS BETWEEN PATTERNS AND PROCESSES

Remote sensing data provide a unique perspective for analysis of modern carbonate depositional systems. As such, they can contribute to qualitative and quantitative insights into patterns and the controlling processes. For example, on the thematic map, mangrove pond subfacies occurs as a ''halo'' between and around the tidal channels of the Three Creeks area (Fig. 2). Open ponds and low algal marshes appear to flank this area on the south, east, and north (to the east are beach ridges and the open marine subfacies). This distribution seems reasonable, because the sediment source is offshore and sediment is transported to the tidal flats through the channels

←

FIG. 2.—**A)** Ultra-high resolution (4 m) remote sensing image (RGB = near infrared, green, blue bands) of part of the study area (image copyright SpaceImaging.com). Aerial photographs (graciously provided by Lawrie Hardie) and 1-m-resolution panchromatic satellite images also were used for comparison. **B)** Landsat TM RGB (bands 3, 2, 1) color image of study area. Black rectangle encloses the area of Part A. **C)** Classified image from study area. Each color represents a spectrally distinct class, interpreted to represent a depositional subfacies. Black square is area of Part A. Note that there is a good relationship between spectral classes and subfacies that can be observed on remote-sensing image and aerial photographs.

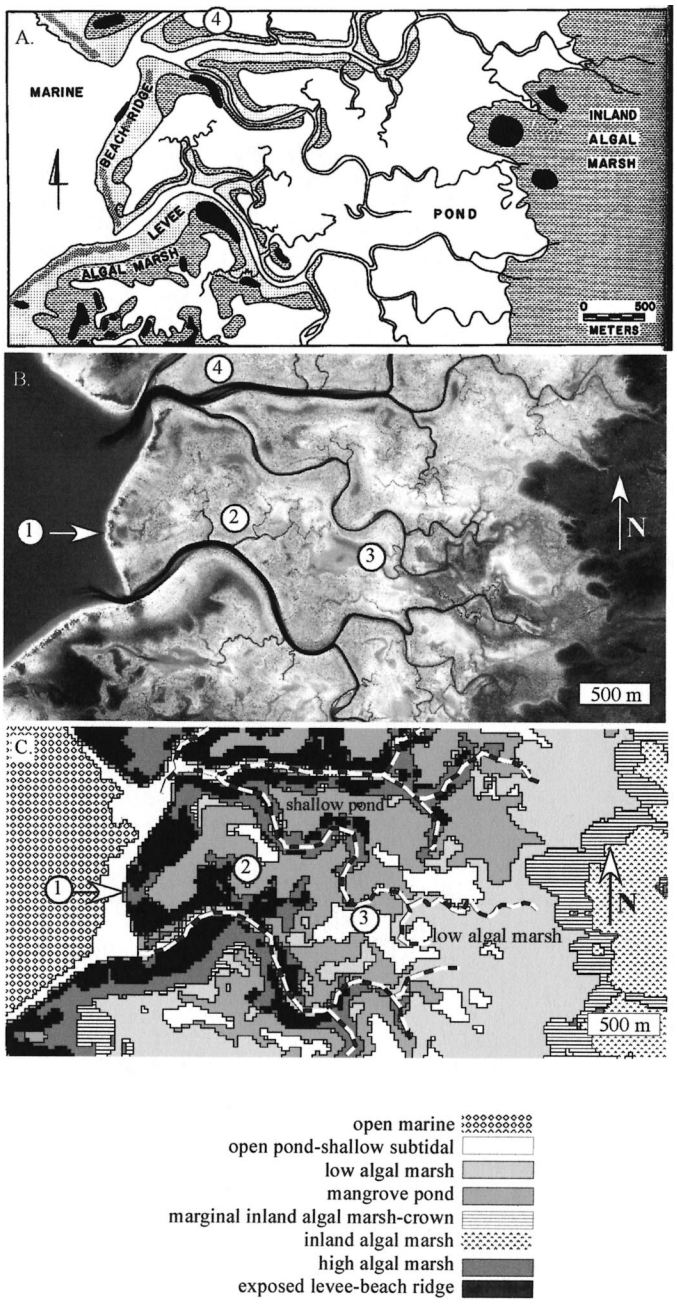

FIG. 3.—Explicit comparison of: **A)** ground-truthed map (Hardie 1977), **B)** ultra-high resolution (1 m) satellite image (acquired 2001, image copyright SpaceImaging.com), and **C)** thematic map sediment accumulations. The thematic map appears in some areas to capture subfacies at a level of detail greater than the Hardie (1977) map, and are consistent with subfacies that would be interpreted from the satellite image (B). Several areas are highlighted: (1) a break in the beach ridge, illustrated in Part B, and present in the classified image; (2) two smaller channels, present on the high-resolution satellite image, but below the resolution of the Landsat data; although the channels are not explicitly distinguished by the classification, it does separate out levee subfacies in this area, showing that the effects of the channels are detected, even if the channels are not resolved; (3) open-pond subfacies clearly visible on the high-resolution imagery (as ''smoother'' texture) and present on the classified image; (4) an example of an area in which the tidal flat has changed between 1943 (when the aerial photos utilized by Hardie and co-workers were taken), the early 1970s (when Hardie et al. worked in the area), 1986 (when the Landsat data were acquired) and 2001 (when the high-resolution image was acquired). The earlier data show an algal marsh (darker colored, identified by Hardie et al.) just to the west of the number 4, but these are absent by 1986 and 2001 (hence do not appear on the classified map). Detailed comparison of the 1943 aerial photos and the 2001 satellite data illustrate that several areas had changed (Rankey and Morgan 2002).

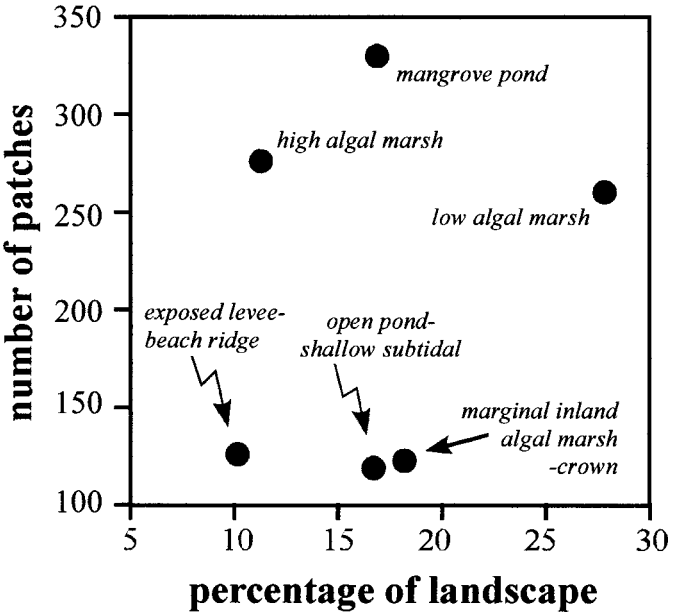

FIG. 4.—Cross plot of number of patches versus total percentage of landscape for each subfacies. Percentage of landscape excludes the inland algal marsh and the open-marine subfacies, and thus includes only channeled-belt subfacies. Note that number of patches does not correlate with percentage of landscape. See text for detailed discussion.

(Shinn et al. 1969). These channeled regions have likely built up slightly higher because of their proximity to the channels, yet this pattern was not described by Shinn et al. (1969) or Hardie (1977).

Similarly, by integrating the remote-sensing analyses in a GIS, the patterns of sediment accumulation can be quantitatively described and tested against sedimentologic insights. For example, given that levees and beach ridges are limited to the flanks of sinuous, but continuous, channels and the shoreline, we might expect that they cover fairly large areas (narrow, but long) but have complex shapes (Fig. 2) that are clumped together (e.g., around channels). Indeed, the data presented herein reveal that exposed levee-beach ridges have low fractal dimension ($D = 1.49$; ''larger'' area), high shape complexity (mean ICC = 0.57, mean long axis : short axis ratio of 2.93), and are separated by gaps that are large and variable ($D = 1.67$ for lacunarity data), consistent with the qualitative sedimentologic prediction. Similarly, open ponds are larger, more circular objects with irregular edges (Fig. 2). Quantitatively, they have larger mean patch area ($D = 1.50$) and fairly high shape complexity (mean ICC = 0.57, mean long axis : short axis ratio of 2.49), consistent with qualitative predictions.

Unique insights on patterns and processes also arise from the quantitative analysis of the entire system. On this tidal flat, characteristics of patch area and gaps between patches showed scale-invariant (fractal) patterns across several orders of magnitude. In the earth sciences, many examples of spatial and/or temporal fractal structures have been described, ranging from river networks to coastlines to earthquake recurrence frequency (Turcotte 1997). Many fractal systems are self-organized (Turcotte 1997; Rodriguez-Iturbe and Rinaldo 1997; Camazine et al. 2001), meaning that ''. . . pattern at the global level of a system emerges solely from numerous interactions among the lower level components of the system . . . executed using only local information, without reference to the global pattern'' (Camazine et al., 2001 p. 8). In other words, the patches do not ''communicate'' with one another to carry out a ''master plan'' in which their sizes and distribution are prescribed or predetermined, but rather the pattern emerges at the global level from the underlying dynamics of the system. Hence, in self-organized systems, ''. . . simple variables arise at the large scale which are not in

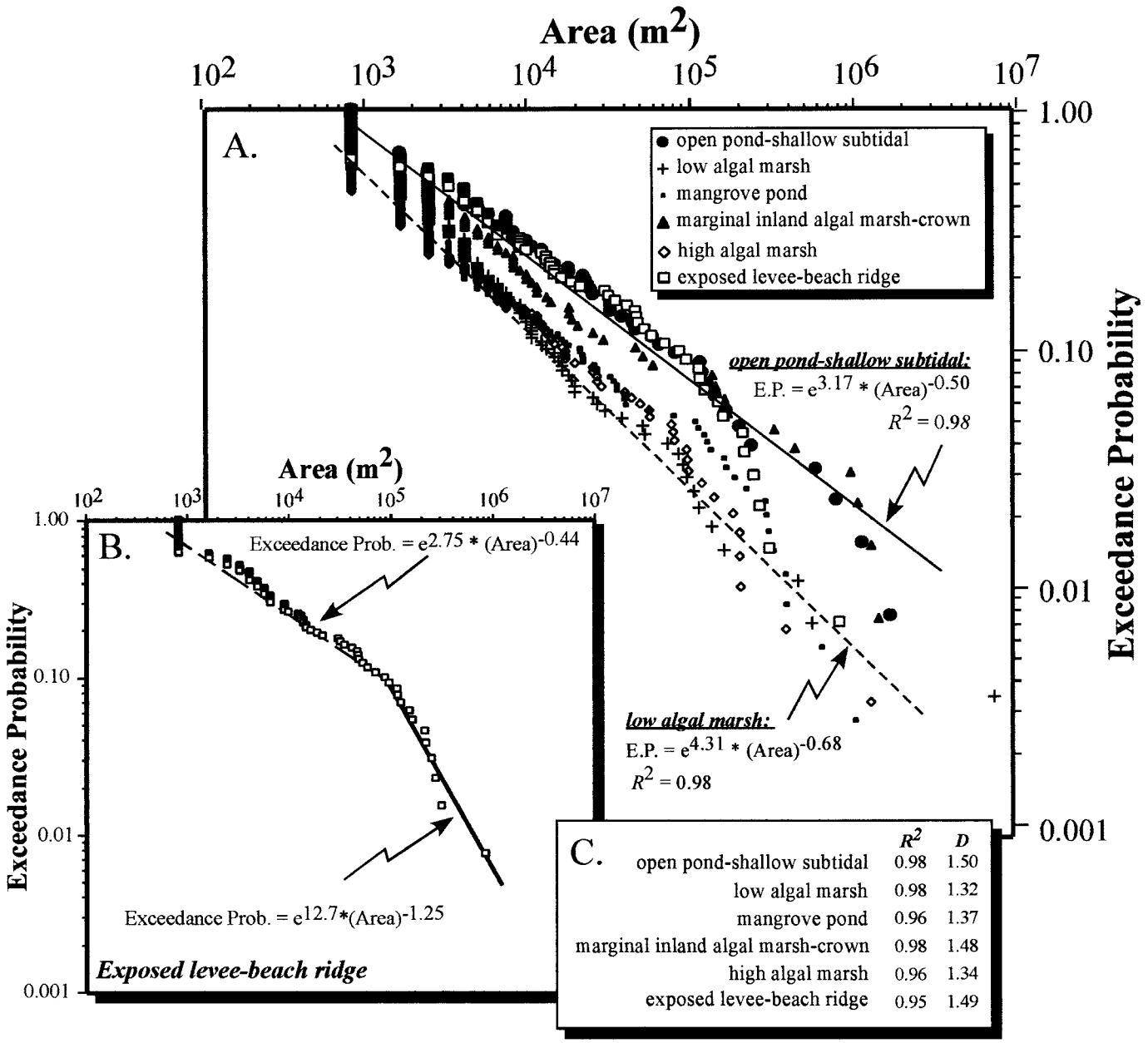

FIG. 5.—Characteristics of patch size by subfacies, illustrated in cross plots of exceedance probability versus area, both on log scales. **A)** Data for all subfacies, illustrating the power-law relationship between these parameters. The two end-member best-fit power laws with smallest and largest slope are illustrated. E.P. = exceedance probability. **B)** Data for the exposed levee-beach ridge subfacies, illustrating the possible presence of bifractal characteristics (Turcotte 1997) or a change in the trend of the data at ~ 10^5 m^2. **C)** Fractal dimension (D) goodness of fit of data plotted in Part A. Goodness-of-fit for power laws relating area-exceedance probability for each subfacies measured by coefficient of determination (R^2) values (cf. Carlson and Grotzinger 2001).

practice derivable from the small scale where simple physics does operate'' (Haff 1997, p. 355).

To explore how fractal characteristics and self-organization might occur, it is informative to place subfacies in a geographic context and apply sedimentologic understanding. Qualitatively, it is evident that smaller patches occur near channels (cf. Fig. 2). In contrast, the largest patches ($> 10^6$ m^2) occur either as environmental end members outside of the channeled belt (inland algal marsh and open marine patches) or away from the main tidal channels and beach ridges, most commonly as open ponds and the low algal marsh. These relations can be quantified by comparing mean distance to channel and mean patch area for subfacies; such analysis illustrates a distinct positive correlation ($R^2 = 0.87$; Fig. 8). Hence, patch size is related to proximity of channels.

On this tidal flat, Hardie (1977) noted rapid lateral environmental changes near channels that led to abrupt facies changes. The channel flanks are the location of the most pronounced lateral changes in elevation (e.g., from channel centers up to levee crests down to high algal marsh and pond), a gradient that leads to rapid lateral changes in environment and facies. Conversely, larger patches (e.g., open marine or inland algal marsh) occur in areas with more homogeneous environmental conditions (lower ''environmental gradients'') at the environmental ''edges'' of the tidal flat—the updip and downdip extremes of the tidal flat system.

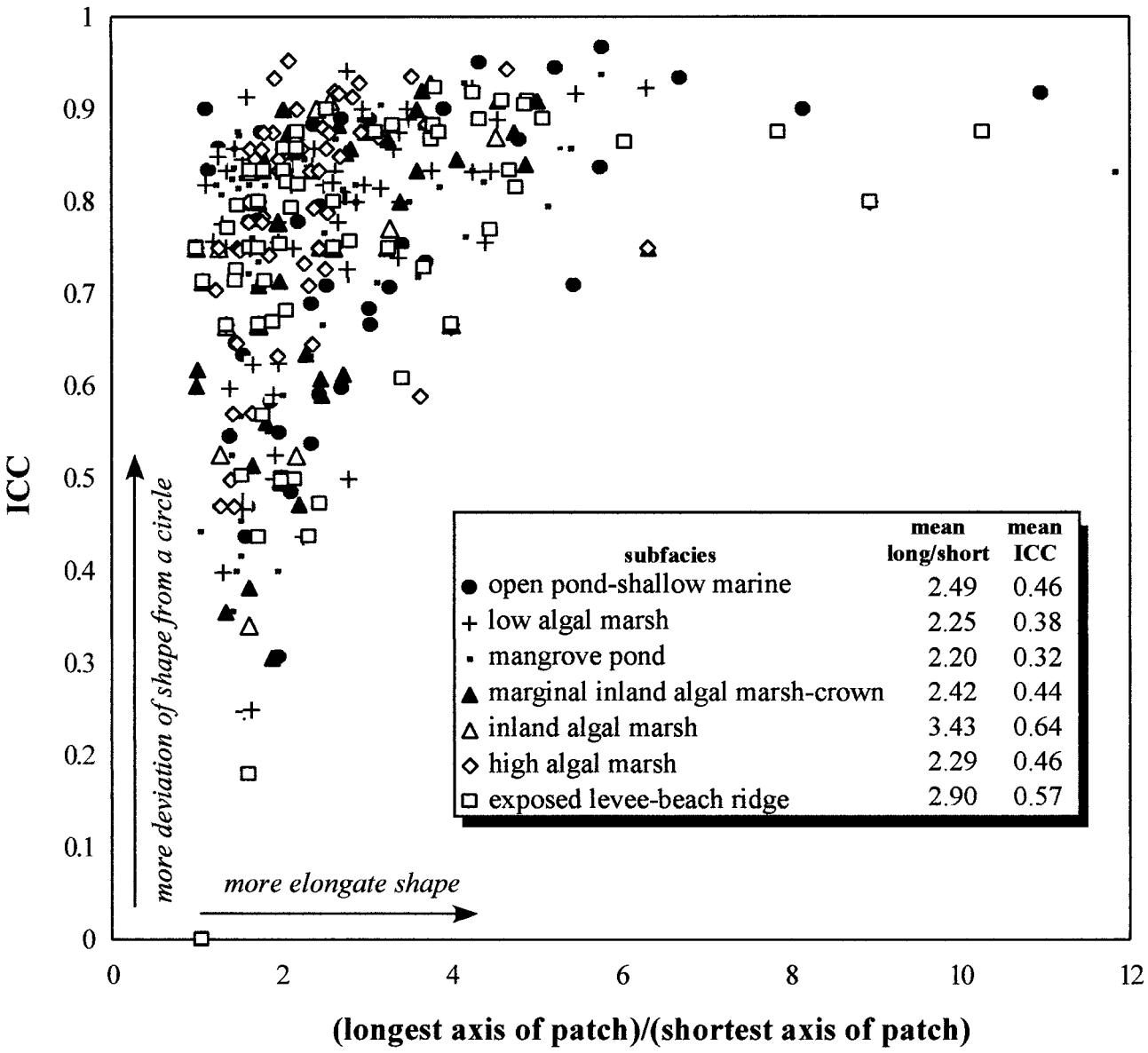

FIG. 6.—Characteristics of patch shape complexity, illustrated by a plot of the ratio of longest axis across a patch to the shortest axis across a patch versus ICC for all patches of each subfacies. For channeled-belt subfacies, the exposed levee-beach ridge has the highest mean ratio, or the most elongate shape. The patches of exposed levee-beach ridge and open pond-shallow subtidal subfacies have the highest mean ICC, indicating their shape (on average) deviates most from a circle. See text for discussion.

In summary, the close relation between proximity to channels and patch area suggests that the two parameters are linked, perhaps through cause and effect as suggested by sedimentologic understanding. How might these interact to create the statistical fractal heterogeneity and self-organization? At the largest scale, the net offshore slope away from Andros Island leads to ''orderly'' environmental changes (from dry land to the inland algal marsh to the channeled belt to shallow marine subfacies). Within this larger-scale gradient are smaller-scale changes in gradient, such as the topographic changes from the levees to the ponds, which may include up to 60 cm relief across several 100 m, and still more subtle changes (e.g., centimeter-scale features related to individual sediment bodies such as storm washover lobes). Intuitively, there would be many more very subtle gradients than larger gradients, and these might be described by a power-law relationship (Turcotte 1997; Rodriguez-Iturbe and Rinaldo 1997). Perhaps it is the continuum in magnitudes of the topographic gradients, through its influence on the size of each individual patch, which leads to the statistical self-similarity that is clearly apparent on the tidal flat at the systemic scale.

CONCLUDING COMMENTS AND QUESTIONS

In recent years, many ancient peritidal successions have been interpreted in the framework of allocyclic processes (for example, Goldhammer et al. 1987; Read and Goldhammer 1988; Koerschner and Read 1989; Goldhammer et al. 1993; Osleger and Read 1993; Yang et al. 1995; Lehrmann and Goldhammer 1999). Due homage has been paid to ideas and models of autogenic processes of carbonate accumulation, however, most commonly on the basis of studies of modern tidal-flat accumulations like those on Andros Island (Ginsburg 1971; Shinn et al. 1969; Hardie and Shinn 1986). In applying these models to ancient successions, and on the basis of interpretations that ''facies successions are more or less random'' (Wilkinson

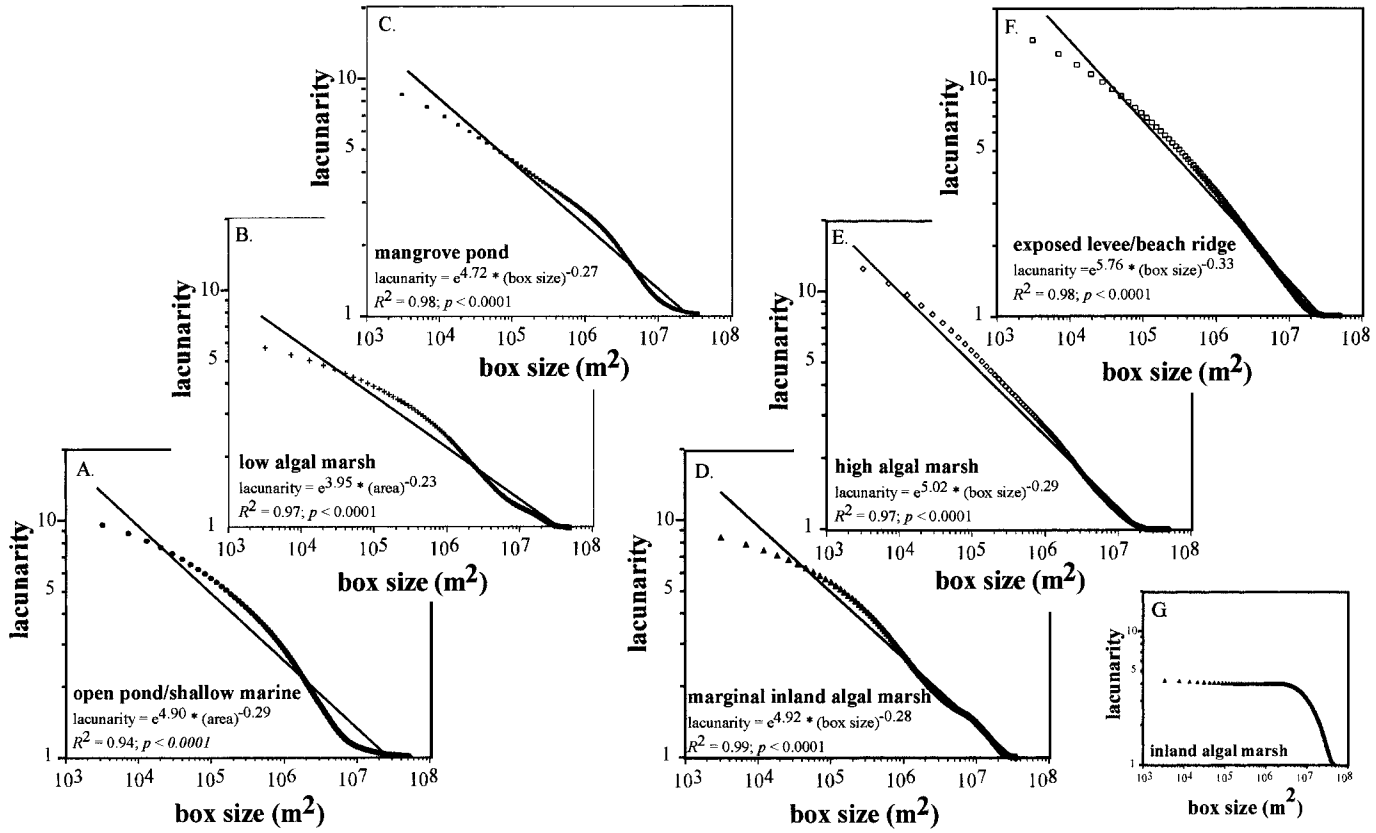

FIG. 7.—Lacunarity plots for all subfacies (A–G). Lacunarity measures the ''gappiness'' of a geometric structure, and power-law relationships between box size and lacunarity are evident. The data for the exposed levee-beach ridge (F) and high algal marsh (E) fall closest to a straight line (a perfect power law) over all scales, consistent with scale-invariant (fractal) characteristics, whereas the data for the inland algal marsh (G) do not. Lacunarity curves for all channeled belt subfacies approximate a straight line across all scales (e.g., exposed levee-beach ridge) or a subset of scales (e.g., 10^3–10^6 for mangrove pond). See text for discussion.

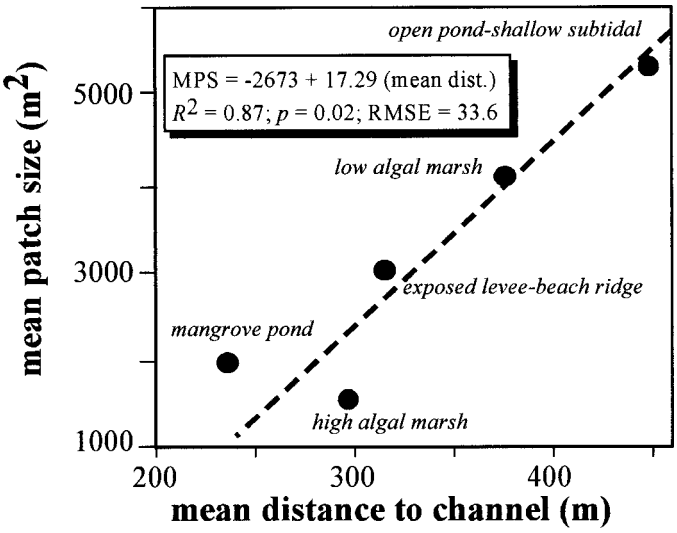

FIG. 8.—Relation between mean patch size (MPS) and mean distance from channel (mean dist.) for each class. Two subfacies, the marginal inland algal marsh-crown and the inland algal marsh, include no large channels and are not influenced significantly by them, and have been excluded from the analysis. For this analysis, channels were identified from the Landsat data (cf., Fig. 2), and therefore include only larger channels. There is a close positive correlation between the two parameters (R^2 = 0.87; RMSE = 33.6 m), consistent with the qualitative observations and sedimentologic interpretations of maximum rate of change in sedimentologic character near the channels.

et al. 1997), some stratigraphers have inferred the influences of ''stochastic processes of sediment accumulation'' (Drummond and Wilkinson 1993) and ''that the nature of lateral (and resultant vertical) transitions may be exceedingly complex'' (Wilkinson et al. 1997). Part of the challenge in interpreting these successions is related to our inability to evaluate the inherent complexity of sedimentary systems (the ''noise'' of the system of Adams and Grotzinger 1996) so that we can isolate the external forcing mechanisms (the ''signal'' of these systems; Adams and Grotzinger 1996).

Whereas the results of this study suggest that while the spatial characteristics of facies patterns and shapes may be complex, they are definitively not random (cf. Figs. 2C, 4–9). This non-randomness is clear in terms of subfacies areas, gaps between subfacies, and lateral transitions between subfacies. If, *at the facies scale,* ancient successions are the result of lateral migrations of facies, and if Walther's Law is valid, why then are detailed vertical facies transition and thickness patterns in many ancient peritidal successions apparently random (e.g., Wilkinson et al. 1997, 1999; Lehrmann and Goldhammer 1999)?

One hypothesis is that some of these ancient successions may not be directly analogous to the Andros channeled belt (e.g., Pratt and James 1986; Satterley 1996). One difference is scale: many ancient peritidal carbonate platforms (for example, the extensive Cambro–Ordovician carbonate platforms of the Appalachians) covered significantly larger areas and had lower gradients. The attributes of self-similarity on the Three Creeks tidal flat suggest that the system has statistically similar characteristics across a range of scales. Therefore, even if larger in scale, analogous channeled systems might show similar nonrandom patterns. (This statement does not imply that ancient facies would by necessity be of the same size as those on the Three Creeks tidal flat, however.)

A second hypothesis that ancient successions may appear more random is due to the lack of fidelity in the stratigraphic record. Past studies (most notably Sadler 1981; cf. Plotnick 1986) have suggested that the stratigraphic record is an incomplete recorder of geologic history and preserves a record of only 10–20% of the duration of a given time period. In this light, the patterns of accumulation on the Holocene tidal flat may not represent the sediments that will be preserved in the final record. This hypothesis is given extra significance upon consideration that the shoreline in this area of northwestern Andros Island is presently being eroded—so none of this tidal flat may actually be preserved! At some point, however, ancient tidal flat deposits were preserved, and there is no *a priori* reason to suspect that they are not highly organized.

A final hypothesis for the increased apparent randomness in ancient successions may be related to the presence of external forcing: instead of representing the ''signal,'' these forces may instead be reflected in the ''noise'' of the system. If the facies patterns of ancient tidal flats were highly organized and nonrandom, then perhaps it is relative changes in sea level that lead to reorganizations of the depositional system. These reorganizations would lead to more randomness in the record by creating vertical facies transitions that are not reflective of laterally adjacent environments and facies areas or transitions that might be out of ''equilibrium'' with gradients. Such changes would appear in vertical sections as deviations from the highly ordered system of the tidal-flat surface, and contribute to apparent randomness.

If this hypothesis is correct, it may be prudent to reconsider what is ''signal'' and what is ''noise'' in ancient peritidal successions. It may be that we have had it backwards: more random facies patterns actually may be the stratigraphic manifestation of the more pronounced influence of external forcing mechanisms overwhelming the ordered internal signal, rather than being the result of migration of a complex suite of randomly distributed depositional subenvironments.

ACKNOWLEDGMENTS

Thanks to Dan Ashlock, Paul Enos, Tom Jones, Dan Lehrmann, Mark Longman, Roy Plotnick, Gene Shinn, Lynn Watney, and Bruce Wilkinson for helpful discussions. Bob Demicco, Mike Kozar, Dan Lehrmann, John Tipper, and Lynn Watney provided thoughtful reviews of this manuscript. Bruce Wilkinson provided considerable commentary and provided a thorough critical discussion of the manuscript that significantly improved and clarified the notions herein. Kent Vander Velden wrote the Markov chain and lacunarity analysis programs used in this project and provided important feedback at key points. Acknowledgment is made to the Donors of the Petroleum Research Fund, administered by the American Chemical Society, and the National Aeronautics and Space Administration (NASA) for support of this research.

REFERENCES CITED

Adams, R.D., and Grotzinger, J.P., 1996, Lateral continuity of facies and parasequences in Middle Cambrian platform carbonates, Carrara Formation, southeastern California, U.S.A.: Journal of Sedimentary Research, v. B66, p. 1079–1090.

Allain, C., and Cloitre, M., 1991, Characterizing the lacunarity of random and deterministic fractal sets: Physical Review A, v. 44, p. 3552–3558.

Andrefouet, S., and Claereboudt, M., 2000, Objective class definitions using correlation of similarities between remotely sensed and environmental data: International Journal of Remote Sensing, v. 21, p. 1925–1930.

Bryson, N., and Mobolurin, A., 2000, Towards modeling the query processing relevant shape complexity of 2D polygonal spatial objects: Information and Software Technology, v. 42, p. 357–365.

Camazine, S., Deneubourg, J., Franks, N.R., Sneyd, J., Theraulaz, G., and Bonabeau, E., 2001, Self-Organization in Biological Systems: Princeton, New Jersey, Princeton University Press, 538 p.

Carlson, J., and Grotzinger, J.P., 2001, Submarine fan subenvironment inferred from turbidite thickness distributions: Sedimentology, v. 48, p. 1331–1351.

Carr, T.R., 1982, Log-linear models, Markov chains, and cyclic sedimentation: Journal of Sedimentary Petrology, v. 52, p. 905–912.

Cloyd, K.C., Demicco, R.V., and Spencer, R.J., 1990, Tidal channel, levee, and crevasse-splay deposits from a Cambrian tidal channel system: A new mechanism to produce shallowing-upward sequences: Journal of Sedimentary Petrology, v. 60, p. 73–83.

Davis, J.C., 1986, Statistics and Data Analysis in Geology: New York, Wiley, 646 p.

Drummond, C.N., and Wilkinson, B.H., 1993, Aperiodic accumulation of cyclic peritidal carbonate: Geology, v. 21, p. 1023–1026.

Enos, P., 1977, Holocene sediment accumulation of south Florida shelf margin, *in* Enos, P., and Perkins, R.D., eds., Quaternary Sedimentation in South Florida: Geological Society of America, Memoir 147, p. 1–130.

Enos, P., 1974, Surface sediment facies of the Florida–Bahamas platform: Geological Society of America, Map and Chart Series MC-5.

Farina, A., 1998, Principles and Methods in Landscape Ecology: Cambridge, U.K., Chapman & Hall, 235 p.

Gebelein, C.D., 1974, Guidebook for Modern Bahamian Platform Environments: Geological Society of America, Annual Meeting, Miami, Florida, Field Trip Guide, 93 p.

Ginsburg, R.N., 1971, Landward movement of carbonate mud: new model for regressive cycles in carbonates (abstract): American Association of Petroleum Geologists Bulletin, v. 55, p. 340.

Gischler, E., and Lomando, A.J., 1999, Recent sedimentary facies of isolated carbonate platforms, Belize–Yucatan system, Central America: Journal of Sedimentary Research, v. 69, p. 748–763.

Goldhammer, R.K., Oswald, E.J., and Dunn, P.A., 1993, Hierarchy of stratigraphic forcing: Example from Middle Pennsylvanian shelf carbonates of the Paradox basin, *in* Franseen, E.K., Watney, W.L., Kendall, C. and Ross, W., eds., Sedimentary Modeling: Computer Simulations and Methods for Improved Parameter Definition: Kansas Geological Survey, Bulletin 233, p. 361–415.

Goldhammer, R.K., Dunn, P.A., and Hardie, L.A., 1987, High-frequency glacio-eustatic sea-level oscillations with Milankovitch characteristics recorded in Middle Triassic platform carbonates in northern Italy: American Journal of Science, v. 287, p. 853–892.

Haff, P.K., 1997, Limitations on predictive modeling in geomorphology, *in* Rhoads, B.L., and Thorn, C.E., eds., The Scientific Nature of Geomorphology: New York. Wiley & Sons, p. 337–358.

Hardie, L.A., ed., 1977, Sedimentation on the modern carbonate tidal flats of northwest Andros Island, Bahamas: Johns Hopkins University, Studies in Geology, no. 22, 202 p.

Hardie, L.A., 1986, Ancient carbonate tidal-flat deposits: Colorado School of Mines Quarterly, v. 81, p. 37–57.

Hardie, L.A., and Shinn, E.A., 1986, Tidal flats, *in* Carbonate Depositional Environments, Modern and Ancient: Colorado School of Mines Quarterly, v. 81, 74 p.

Hardie, L.A., Dunn, P.A., and Goldhammer, R.K., 1991, Field and modeling studies of Cambrian carbonate cycles, Virginia Appalachians—Discussion: Journal of Sedimentary Petrology, v. 61, p. 636–646.

Harris, P.M., 1979, Facies anatomy and diagenesis of a Bahamian ooid shoal: University of Miami, Comparative Sedimentology Laboratory, Sedimenta VII, 163 p.

Harris, P.M., and Kowalik, W.S., 1994, Satellite images of carbonate depositional settings: examples of reservoir- and exploration-scale geological facies variation: American Association of Petroleum Geologists, Methods in Exploration Series, no. 11, 147 p.

King, A.W., 1987, Translating models across scales in the landscape, *in* Turner, M.G., and Gardner, R.H., eds., Quantitative Methods in Landscape Ecology: Berlin, Springer-Verlag Ecological Studies, no. 82, p. 479–517.

Kozar, M.G., Weber, L.J., and Walker, K.R., 1990, Field and modeling studies of Cambrian carbonate cycles, Virginia Appalachians—Discussion: Journal of Sedimentary Petrology, v. 60, p. 790–794.

Koerschner, W.F. III, and Read, J.F., 1989, Field and modeling studies of Cambrian carbonate cycles, Virginia Appalachians: Journal of Sedimentary Petrology, v. 59, p. 645–659.

Laporte, L.F., 1967, Carbonate deposition near mean sea-level and resultant facies mosaic: Manlius Formation (Lower Devonian) of New York state: American Association of Petroleum Geologists, Bulletin, v. 51, p. 73–101.

Lehrmann, D.J., and Goldhammer, R.K., 1999, Secular variation in parasequence and facies stacking patterns of platform carbonates: A guide to the application of stacking-pattern analysis in strata of diverse ages and settings, *in* Harris, P.M., Saller, A.H., and Simo, J.T., eds., Recent Advances in Carbonate Sequence Stratigraphy: Applications to Reservoirs, Outcrops, and Models: SEPM, Special Publication 63, p. 187–226.

McNeill, D.F., 1998, Dimensional aspects of Holocene pinnacle reefs in a mixed carbonate siliciclastic system, southern Belize lagoon: University of Miami, Comparative Sedimentology Laboratory, unpublished report, 47 p.

Obeysekera, J., and Rutchey, K., 1997, Selection of scale for Everglades landscape models: Landscape Ecology, v. 12, p. 7–18.

Osleger, D., and Read, J.F., 1993, Comparative analysis of methods used to define eustatic variations in outcrop: Later Cambrian interbasinal sequence development: American Journal of Science, v. 293, p. 157–216.

Plotnick, R.E., 1986, A fractal model for the distribution of stratigraphic hiatuses: Journal of Geology, v. 94, p. 885–890.

Plotnick, R.E., Gardner, R.H., and O'Neill, R.V., 1993, Lacunarity indices as measures of landscape texture: Landscape Ecology, v. 8, p. 201–211.

Pratt, B.R., and James, N.P., 1986, The St. George Group (Lower Ordovician) of western Newfoundland: Tidal flat island model for carbonate sedimentation in shallow epiric seas: Sedimentology, v. 33, p. 313–343.

Rankey, E.C., and Morgan, J.J., 2002, Quantified rates of geomorphic change on a modern carbonate tidal flat, Bahamas: Geology, v. 30, p. 583–586.

Read, J.F., and Goldhammer, R.K., 1988, Use of Fischer plots to define third-order sea-level curves in Ordovician peritidal carbonates, Appalachians: Geology, v. 16, p. 895–899.

Rodriguez-Iturbe, I, and Rinaldo, A., 1997, Fractal River Basins: Chance and Self-Organization: Cambridge, U.K., Cambridge University Press, 547 p.

Rodriguez-Iturbe, I., Ijjasz-Vasquez, R., Bras, R.L., and Tarboton, D.G., 1992, Power-law distribution of mass and energy in river basins: Water Resources Research, v. 28, p. 988–993.

SADLER, P.M., 1981, Sediment accumulation rates and the completeness of stratigraphic sections: Journal of Geology, v. 89, p. 569–584.

SATTERLEY, A.K., 1996, Cyclic carbonate sedimentation in the Upper Triassic Dachstein Limestone, Austria: the role of patterns of sediment supply and tectonics in a platform-reef-basin system: Journal of Sedimentary Research, v. B66, p. 307–323.

SAURA, S., AND MARTINEZ-MILLAN, J., 2001, Sensitivity of landscape pattern metrics to spatial extent: Photogrammetric Engineering and Remote Sensing, v. 67, p. 1027–1036.

SHINN, E.A., 1973a, Recent intertidal and nearshore carbonate sedimentation around rock highs, E. Qatar, Persian Gulf, *in* Purser, B.H., ed., The Persian Gulf: New York, Springer-Verlag, p. 193–198.

SHINN, E.A., 1973b, Sedimentary accretion along the leeward, SE coast of Qatar peninsula, Persian Gulf, *in* Purser, B.H., ed., The Persian Gulf: New York, Springer-Verlag, p. 199–210.

SHINN, E.A., LLOYD, R.M., AND GINSBURG, R.N., 1969, Anatomy of a modern carbonate tidal flat, Andros Island, Bahamas: Journal of Sedimentary Petrology, v. 39, p. 1202–1228.

TURCOTTE, D.L., 1997, Fractals in Geology and Geophysics: Cambridge, U.K., Cambridge University Press, 397 p.

TURNER, M.G., AND GARDNER, R.H., 1991, Quantitative Methods in Landscape Ecology: Berlin, Springer-Verlag Ecological Studies 82, 536 p.

WATERS, B.B., SPENCER, R.J., AND DEMICCO, R.V., 1989, Three-dimensional architecture of shallowing-upward carbonate cycles: Middle and Upper Cambrian Waterfowl Formation, Canmore, Alberta: Bulletin of Canadian Petroleum Geology, v. 37, p. 198–209.

WILKINSON, B.H., DRUMMOND, C.N., DIEDRICH, N.W., AND ROTHMAN, E.D., 1999, Poisson processes of carbonate accumulation on Paleozoic and Holocene platforms: Journal of Sedimentary Research: v. 69, p. 338–350.

WILKINSON, B.H., DRUMMOND, C.N., ROTHMAN, E.D., AND DIEDRICH, N.W., 1997, Stratal order in peritidal carbonate sequences: Journal of Sedimentary Research, v. 67, p. 1068–1082.

YANG, W., HARMSEN, F., AND KOMINZ, M.A., 1995, Quantitative analysis of a cyclic peritidal sequence, the Middle and Upper Devonian Lost Burro Formation, Death Valley, California—A possible record of Milankovitch climatic cycles: Journal of Sedimentary Research, v. 65, p. 306–322.

Received 9 May 2001; accepted 7 February 2002.